# Time-resolved electron temperature of a low power Hall thruster

Mary F. Konopliv\* and Richard E. Wirz<sup>†</sup> University of California: Los Angeles, Los Angeles, CA, 90095, USA

Lee K. Johnson<sup>‡</sup>

Jet Propulsion Laboratory, California Institute of Technology, La Canada Flintridge, CA, 91011, USA

Time-dependent behavior of electrons can be critically important to Hall thruster discharge behavior. Fast Optical Emission Spectroscopy (FastOES) is a non-invasive diagnostic capable of measuring the time-resolved electron temperature of the plasma. The FastOES approach splits the collected light and isolates two distinct wavelengths that are detected by photomultiplier tubes, and amplified to a measurable signal. These measured emission lines are paired with a collisional-radiative model to determine time-resolved electron temperature. Using this technique, the FastOES results show that the electron temperature exhibits both temporal and spatial variations within the Hall thruster. There is a dynamic relationship between the electron temperature and the discharge current, with the electron temperature consistently exhibiting an out-of-phase relationship in correlation with the discharge current. Additionally, a loose scaling relationship was identified, providing valuable insights into the complex interplay within Hall thruster plasmas.

## I. Nomenclature

 $\alpha$  = ratio of singly charged ion number density to electron number density

 $\omega$  = frequency of breathing mode oscillations

 $\chi^2$  = average squared residual

 $A_{jk}$  = Einstein coefficient for the spontaneous emission transition from level j to k

 $E_k$  = energy of state k

 $I_D$  = Anode discharge current J = emission line intensity

K = rate coefficient for transitions indicated by the subscript

 $L_{iz}$  = length of ionization region

 $n_e$  = electron density

 $n_k$  = population density of xenon ions excited to state k

 $T_e$  = electron temperature

 $u_i$  = ion velocity  $u_n$  = neutral velocity

 $V_D$  = Anode discharge voltage

## **II. Introduction**

Hall thrusters, a popular electric propulsion technology, have gained prominence for in-space propulsion due to their high specific impulse and efficiency, making them ideal for applications like satellite station keeping or longer deep space missions. Decades of research have gone into investigating the plasma physics of Hall thruster plumes through a combination of modeling and experimental work in vacuum facilities. The obtained experimental results help to give confidence to underlying assumptions in simplified models, with a goal of advancing predictive modeling for Hall thrusters. To enhance our understanding of the intricate nature of Hall thrusters and further advance the technology, it is vital to understand the many phenomena and oscillations commonly observed in the plasma discharge of Hall thrusters.

<sup>\*</sup>PhD Candidate, Mechanical and Aerospace Engineering, mkonopliv@ucla.edu

<sup>†</sup>Professor, Mechanical and Aerospace Engineering, AIAA Associate Fellow, wirz@ucla.edu

<sup>&</sup>lt;sup>‡</sup>Technologist, Electric Propulsion, lee.k.johnson@jpl.nasa.gov

One such oscillation is the breathing mode, a low-frequency global oscillation on the order of 10's of kHz frequently observed in the discharge current of Hall thrusters. The presence and nature of the breathing mode serves as an indicator of Hall thruster health and plays a role in assessing whether operations are within expected parameters. Furthermore, these oscillations are commonly used as calibration criteria in Hall thruster modeling. This paper focuses on electron temperature oscillations within Hall thrusters, with a specific emphasis on the breathing mode. Historically, models have often assumed a constant electron temperature to streamline mathematical analyses and computational models. However, this simplification deviates from the dynamic nature of Hall thruster plasmas, where electron temperature can exhibit temporal variations. Consequently, our investigation centers on understanding the electron temperature variations associated with the breathing mode.

To explore electron temperature variations, we FastOES, a time-resolved version of optical emission spectroscopy, is utilized. This non-invasive diagnostic leverages the measured time-series of the light emitted from the plasma and collisional-radiative modeling to extract time-resolved temperature. The diagnostic is designed to measure oscillations with frequencies up to 10's of MHz. Although the higher frequency oscillations are difficult to distinguish through the noise of the system, the relatively large amplitude and low frequency breathing mode oscillations in the 10's of kHz are more easily observed. Experiments using this diagnostic have revealed both temporal and spatial variations in electron temperature, an observation explored extensively in Section V. The observed fluctuations underscore the need to assess assumptions regarding the constancy of electron temperature, aiming to enhance the accuracy of Hall thruster models.

The objective of this research effort is to understand the significance of electron temperature variations in the breathing mode and their correlation with the discharge current in Hall thrusters. To do so, we specifically measure and evaluate the amplitude of temporal oscillations in the electron temperature. The results are used to evaluate the phase relationship between electron temperature and the discharge current, along with exploring any scaling relationships between electron temperature and discharge current oscillation amplitudes. We hypothesize that the electron temperature does undergo temporal variations throughout the breathing mode, and that the amplitude of these oscillations scales with the amplitude of the discharge current oscillations. The remainder of this paper provides further background on prior research concerning the breathing mode in Section III, specifically discussing the role of electron temperature oscillations. In Section IV, detailed information is provided on the experimental setup with FastOES and methods used to obtain time-resolved electron temperature. Then, we present the collected data in Section V and a discuss the implications of these results in Section VI. We discuss continued efforts in this research endeavor in Section VIII.

# III. Background

Several attempts have been made to model the breathing mode, with a range of complexity. One more simple model is known as the predator-prey model, initially introduced by Fife et al. [1]. In this model, neutral atoms act as the prey, electrons as predators, and the ionization region in the discharge channel serves as the focal point. A cycle ensues where neutral fill from the anode increases the neutral density in the region, facilitating ionization. Subsequently, neutral density decreases while ion density increases. The accelerated ions lead to a decrease in ion density, enabling a renewed increase in neutral density. The resulting equation for the frequency of predicted oscillations is given by

$$\omega = \frac{\sqrt{u_i u_n}}{L_{iz}} \tag{1}$$

where  $u_i$  is the ion velocity,  $u_n$  is the neutral velocity, and  $L_{iz}$  is the length of the ionization region. While this model provides a plausible and simple explanation of the breathing mode mechanisms, potentially yielding a reasonably accurate prediction of the breathing mode frequency, it has limitations. Specifically, it does not predict growth and relies on defining the ionization length, a parameter that may not be definitively known.

A "two-zone" modification of this theory was introduced by Dale and Jorns [2]. This model incorporates coupled ionization instabilities near the anode and in the conventionally examined ionization region. The consequence of this coupling is that the neutral density entering the ionization region fluctuates, rather than maintaining a constant value. This modification allowed for a prediction of growth in the breathing mode model, which the simpler predator-prey model failed to achieve. In an effort to validate the two-zone model, Dale and Jorns performed an experiment employing a combination of time-resolved laser-induced fluorescence and electrostatic probing [3]. Their findings indicated that the model provided slightly lower, yet still reasonably close frequency predictions compared to the observed breathing mode frequency. While there are still limitations to this model, it appears to be an improvement over the original predator-prey model.

More sophisticated computational models have also been explored. For instance, Barral and Ahedo [4] conducted a

comparison between results obtained from a 1-D linearized low-frequency model and a fully time-dependent numerical model. Raisan et al. [5] developed a 2-D hybrid-direct kinetic simulation, while Hara et al. [6] created a 1-D hybrid-direct kinetic simulation. While these complex computational models potentially offer greater accuracy and excel in predicting a more comprehensive set of plasma parameters, extracting physical explanations or analytical expressions for them is more challenging.

There is also a focused research effort aiming to understand the stability criteria for the breathing mode, i.e. the conditions necessary for its onset and sustenance. Numerous studies have explored the role of electron temperature fluctuations, with an intial suggestion that electron temperature fluctuations are required by Hara et al. in 2014 [7]. However, Dale and Hara et al. later corrected this [8], finding that electron temperature fluctuations could not sustain the breathing mode oscillations. Another investigation, utilizing an un-calibrated model, highlighted the significance of both electron temperature fluctuations and non-linearity in electron power absorption [9]. Conversely, a study employing a model calibrated with discharge current breathing mode oscillations found that of the two components influencing electron mobility, neutral density and electron temperature, only neutral density fluctuations were required for the onset and sustenance of the breathing mode [10]. Electron temperature fluctuations alone did not induce breathing mode oscillations. Despite this, the paper acknowledges that electron temperature fluctuations may still hold some significance. The discussion extends to how results change when assuming that the electron temperature fluctuations scale with neutral density fluctuations, and suggests that the reason for breathing mode onset may be case-dependent. Furthermore, the paper notes an expected out-of-phase relationship between electron temperature and neutral density fluctuations.

# IV. Methodology

The overall approach with optical emission spectroscopy (OES) is to collect emitted light from the desired section of plasma, measure the intensities of specific emission lines, and pair those measured intensities with a collisional-radiative model (CRM) to extract plasma parameters, namely electron temperature. Traditionally, a spectrometer with a CCD is used to measure the emission lines in OES. However, to obtain sufficient time resolution with FastOES, photodiodes with a faster time response are used instead. The details of the optical setup are laid out in the following section. This will encompass the collection optic setup and a discussion of the spatial resolution of the diagnostic, a description of the bench-top setup for filtering and measuring the time-resolved emission signals, the CRM used to extract electron temperature via a line-ratio technique, and the method for calibration of the diagnostic.

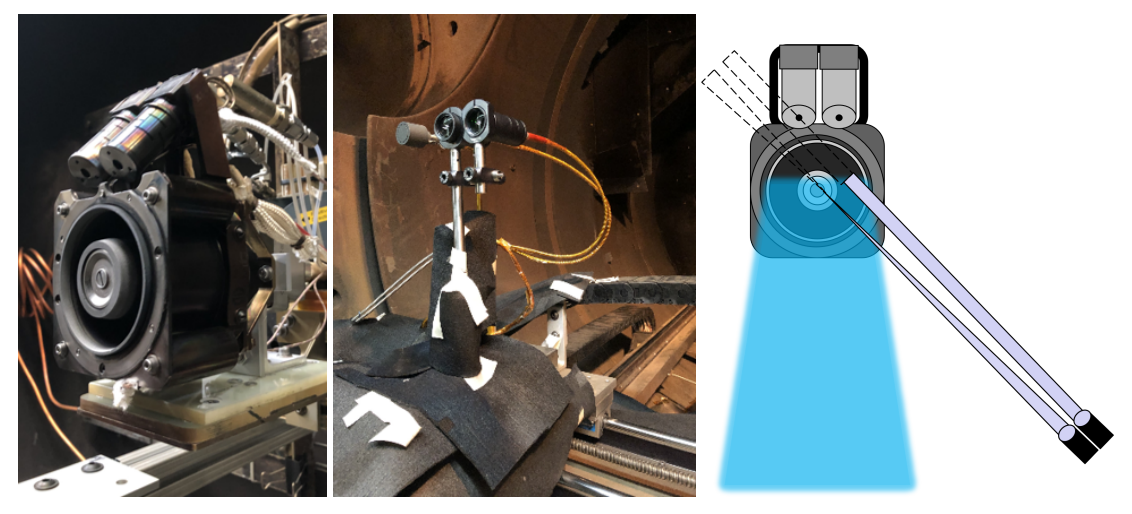
## A. Facility Setup

The experiments were conducted in the "Big Green" vacuum test facility at the Jet Propulsion Laboratory's Electric Propulsion lab[11]. This facility is approximately 2 m wide in diameter and 3.5 m long. There are three diffusion pumps and four cryogenic pumps which can be used to obtain a lower vacuum pressure. During thruster operation, the typical pressures range from  $10^{-5}$  to  $10^{-6}$  torr.

The plasma source for this experiment is a low-power unshielded Hall thruster, the SPT-70. The channel walls of the thruster have a nominal outer diameter of 70 mm, and four external magnetic coils generate a radial magnetic field. The thruster used in this study has two lanthanum hexaboride cathodes, although only one was employed. Nominally, this thruster operates at 660 W, with a discharge voltage of 300 V and a discharge current of 2.2 A. A typical current drawn by the magnet power supply is also about 2.2 A. However, at this nominal condition, the discharge current oscillations are very small amplitude. For this experiment, in order to better study the breathing mode oscillations, the thruster was operated at several combinations of lower power levels and varying magnetic field levels that produced clear breathing mode oscillations in the discharge current.

The thruster was mounted at one end of the Big Green facility, shown in Fig. 1a. Shortly downstream, there is a three-axis  $(X - Y - \theta)$  motion stage on which collection optics are mounted, shown in Fig. 1b. Fibers run from these collection optics to a fiber feedthrough in the back of the chamber. The bench-top setup for FastOES is located outside of the chamber, detailed in Section IV.B. Two collection optics are mounted to the motion stage system. One is a collimated optic, such that the line of sight of the optic is a paraxial beam. The other is a focused collection optic, designed such that the line of sight is conical with a focus point of about 1 mm in diameter located 18.5 mm downstream of the optic. Typical lines of sight of each optic are shown in Fig. 1c.

A common limitation of OES measurements is spatial resolution. As mentioned, the collected light is the sum of everything in the line of sight of the collection optic. One way to provide spatial resolution is to employ mathematical inversions given many paraxial line of sight measurements such as an Abel or Radon transform. This has been used in previous OES experiments[12][13]. Another way to provide at least some semblance of spatial resolution is to employ



(a) Low-power Hall thruster in (b) Collection optics mounted on the (c) Typical line of sight of focused (left) Big Green facility.  $X - Y - \theta$  motion stage downstream. and collimated (right) collection optics.

Fig. 1 Thruster and collection optic setup in the Big Green vacuum facility.

the focused collection optic rather than the collimated collection optic, and to assume that the signal is most concentrated at the focus point of the beam. This assumption seems especially justified if the focus point is located at the brightest part of the plasma. The spatial resolution of this technique can further be enhanced by directing the collection optics to the area of interest off-axis of the thruster as is shown in Fig. 1c to avoid capturing excess background signal in the Hall thruster plume. With the  $X - Y - \theta$  motion stages, it is possible to direct the focused optic at the discharge channel exit at an angle and to scan across the thruster face, thereby obtaining spatially resolved measurements to some extent. Potential methods to further improve spatial resolution of OES measurements are discussed in Section VIII. For the current study, the focused collection optic was positioned at a 45-degree angle, targeting the brightest region of the discharge channel.

#### **B. FastOES Benchtop Setup**

The FastOES diagnostic setup is illustrated in Fig. 2. The process begins with the emission light captured by the in-chamber collection optics being directed out through a fiber optic feedthrough. Subsequently, the light is collimated and split with a beamsplitter designed for near-infrared wavelengths. The transmitted and reflected components of the split light then pass through narrow bandwidth line filters of specific wavelengths to be used with the CRM line-ratio technique. For example, the ratio of intensities of the 823.2 nm and 828 nm emission lines are typically used for analysis of a xenon discharge plume with the neutral xenon (Xe I) CRM, and the filters employed in this experiment are rated for these wavelengths.

Following this, each filtered wavelength is detected by a photomultiplier tube with adjustable gain, and the resulting current output is amplified via high-speed transimpedance amplifier circuits with a gain of  $50,000 \, V/A$  and a bandwidth of 25 MHz. While alternative detectors like avalanche photodiodes could replace the photomultiplier tubes, the latter were chosen for their higher gain, although they have a greater sensitivity to noise, to optimize signal strength in this experiment. Finally, the time-resolved output signal of each wavelength is recorded using a data acquisition system, such as an oscilloscope capable of high-speed measurements. The method for extracting time-resolved electron temperature from this information is outlined in Section IV.C. More specifics of the diagnostic setup are detailed in Ref. [14].

## C. Data Collection and Processing

# 1. Data Acquisition and Averaging

Data was acquired using a Teledyne LeCroy HDO8038A 350 MHz high definition oscilloscope. Three channels were used, with two assigned to each one of the emission lines, and the third dedicated to recording the discharge current. The data was sampled at 20 MHz for a duration of 500 ms, resulting in 50 million data points for each channel. This

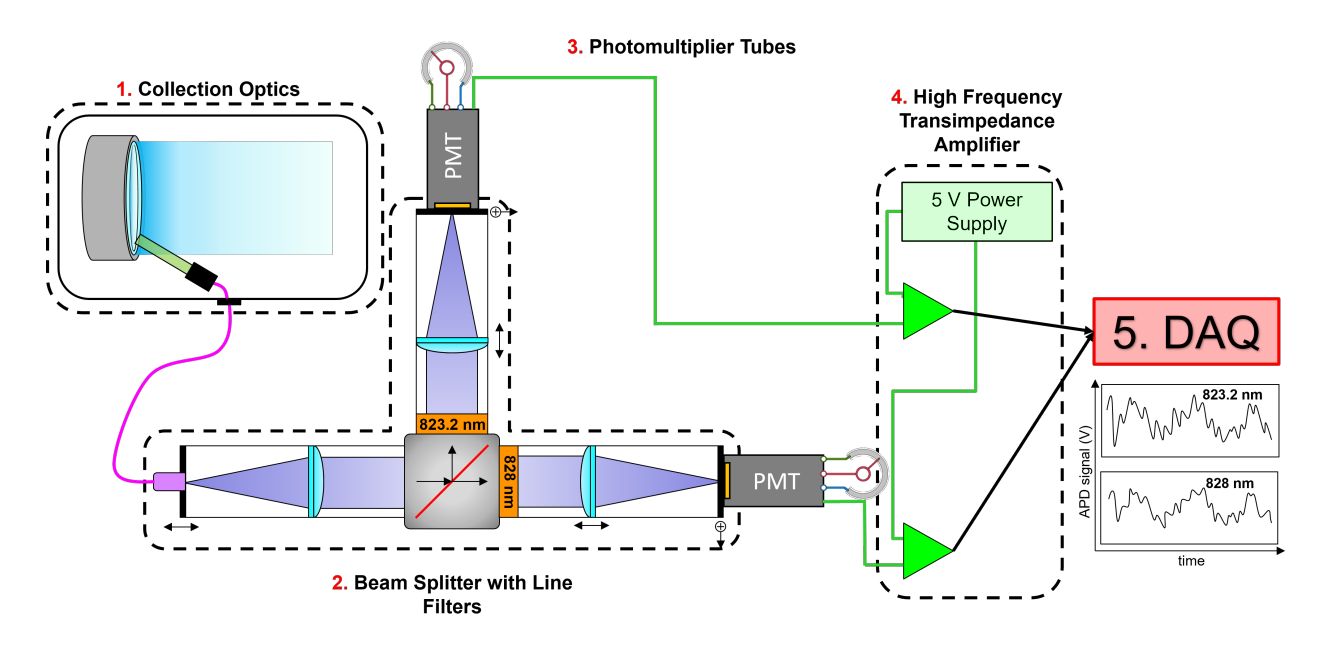


Fig. 2 FastOES bench-top setup.

extensive data collection is intended to facilitate signal statistics, including frequency analysis during post processing. The time-series of the discharge current serves as reference signal that can be correlated to the measured emission lines and resulting time-resolved electron temperature.

The raw time-resolved emission signals often exhibit a high frequency hash-like noise, although the overall signal shape closely follows that of the discharge current time series. This is an anticipated challenge with FastOES, where achieving an acceptable signal-to-noise ratio (SNR) can be difficult. Various sources of noise, such as thermal noise that is not amplified with the signal, shot noise resulting from the variability in the distribution of collected photons from one interval to the next, and noise linked to the transimpedance amplifiers, all contribute to the noise superimposed on the signal. To enhance the clarity of the optical signal, we employ averaging and filtering techniques. Among these, a commonly used and relatively straightforward method is a moving average. It is crucial to strike a balance between averaging enough to smooth the signal and avoid excessive averaging that it may alter its inherent nature. In particular for this study, the goal is to remove the high frequency noise while preserving a clear representation of the low frequency breathing mode oscillations.

Additionally, examining the frequency content of the raw signals is often useful. Applying a fast Fourier transform (FFT) provides insights into the frequency distribution, producing a power spectrum that details the energy associated with a range of frequencies. It is important to note that this technique has limitations, including the loss of local time information when transitioning to the frequency domain. An extension to this approach is the cross-power spectral density (CPSD), unveiling the correlation between two discrete time signals through the comparison of their respective FFTs. This analysis utilizes both FFT and CPSD techniques, and specifically explores the correlation between emission signals and the discharge current.

#### 2. Extracting Electron Temperature with Collisional-Radiative Models

A collisional-radiative (CRM) is used to related the measured emission line intensities to plasma parameters. CRMs in general calculate the population density of the excited states of atoms and ions that result from interactions between the electrons, atoms, and ions in a plasma discharge. The excited states eventually decay to lower a lower energy level, and energy is conserved in this process via the emission of a photon. For decay from upper state k to lower state j, the intensity of the emitted light, J, is given by the density of the upper excited state,  $n_k$ , multiplied by the frequency of decay from the upper to the lower state,  $A_{jk}$ , and multiplied by the difference in energy, E between the upper and lower states:

$$J = n_k A_{ik} (E_k - E_i) \tag{2}$$

To determine the density of the upper excited state  $n_k$ , a steady-state rate equation containing the sum of all

populating and depopulating processes is solved. The rate equation for the Xe I CR model used in this work

$$\frac{dn_k}{dt} = 0 = \left(\sum_{j \neq k} n_e n_j K_{jk} + \sum_{j > k} n_j A_{jk}\right) + n_e n_g \left(K_{gk} + \alpha K_{gk,Xe+} + \frac{1 - \alpha}{2} K_{gk,Xe2+}\right) - \left(\sum_{j \neq k} n_e K_{kj} + n_e K_{kg} - n_e K_{k,iz} - \sum_{j < k} A_{kj} + A_{kg}\right) n_k$$
(3)

where subscript g refers to the ground state of neutral xenon.  $\alpha$  is defined as the ratio of singly-charged ion density,  $n_{i1}$ , to electron density,  $n_e$ . Further details on this model and the populating and depopulating processes accounted for are given in Ref. [15].

In summary, the CRM predicts Xe I emission line intensities based on input parameters such as electron temperature, electron density, neutral density, and others. Utilizing the line ratio of the intensities of two emission lines helps mitigate the influence of factors such as neutral density. The "line ratio" method involves calculating the line ratio produced by the CRM across a range of electron temperatures, assuming a consistent electron density and other plasma parameters. Fig. 3 illustrates generated curves depicting the line ratio between 823.2 nm and 828 nm against electron temperature for various assumed electron densities. The 823.2 nm to 828 nm line ratio has been previously identified as roughly independent of other plasma parameters[16]. If the plasma's electron temperature is roughly known within an order of magnitude, the measured line ratio may be compared to this curve to determine the best-fit electron temperature.

If more than two lines are included in the analysis, which is possible when utilizing a spectrometer to capture the entire spectrum, one can simultaneously determine the electron temperature and electron density. In this multi-line analysis, the best fit electron temperature and density are determined by identifying the inputs to the CRM associated with the set of predicted emission lines that minimizes the average squared residual given in Eqn. 4.

$$\chi^2 = \frac{1}{n} \sum_{i=1}^{n} \frac{(J_i^{meas} - J_i^{CRM})^2}{(J_i^{meas})^2}$$
 (4)

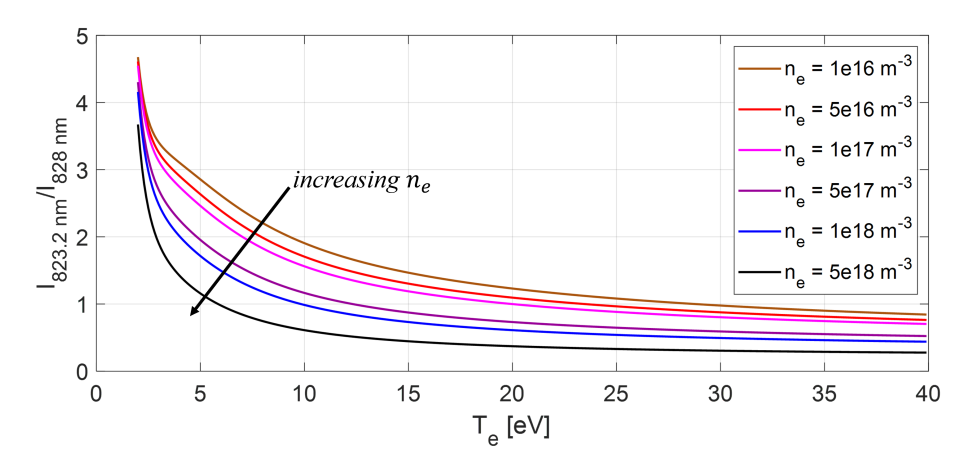


Fig. 3 Line ratio of 823.2 nm to 828 nm versus electron temperature across different electron densities.

It is worth noting that the time resolution of the 823.2 nm to 828 nm line ratio may face limitations. This is attributed to the population of the upper level of the 823.2 nm line by a metastable state, causing the intensity of this emission line to respond to changes in plasma parameters at slower collisional timescales rather than radiative timescales. A study utilizing a time-dependent version of the Xe I CRM, as detailed in Ref. [15], established that the condition for accurate electron temperature measurements with the 823.2 nm to 828 nm line ratio is given by  $f << \frac{n_e}{10^{18}m^{-3}} \cdot (50kHz)$ . For an anticipated electron density of about  $5 \times 10^{17}m^{-3}$ , this threshold would be 25 kHz. The threshold for a slightly lower density of  $1 \times 10^{17}m^{-3}$  would be 5 kHz. The breathing mode frequencies in these experiments ranged between 5 and 15 kHz, so while the time response of the 823.2 nm to 828 nm line ratio is not optimal, it may still fall within an acceptable range.

#### 3. Calibration

To ensure the accuracy of the measured line ratio and thus the resulting electron temperature, a critical step involves the calibration of the FastOES system. This is necessitated by the inherent variability in optical losses across different paths of the beamsplitter, sensitivity of the photomultiplier tubes, and gains of the transimpedance amplifiers. To achieve this calibration, we employ a broadband tungsten lamp for which the intensities of the 823.2 nm and 828 nm lines are approximately equal. By measuring the output of each path under uniform light conditions, we can establish a ratio of losses for each path. This ratio is subsequently used to correct the measured line ratio.

## V. Results

Under the nominal thruster operating conditions, the discharge current oscillations are minimal. To enhance the coherence of the breathing mode oscillation in the discharge current, the thruster operating conditions were adjusted, including the discharge voltage, discharge current, and magnetic field strength. The subsequent sections present findings from three distinct operating conditions that resulted in discharge oscillations of varying frequency, amplitude, and coherence. The results encompass smoothed time-resolved emission signals and the discharge current, the Fast Fourier Transform (FFT) of each signal for frequency analysis, and the corresponding time-resolved electron temperature derived from the 823.2 nm to 828 nm line ratio. Additionally, at each operating condition, spectra were recorded, and the time-averaged electron temperature was calculated. A comparison between the electron temperature obtained from spectra and the mean value of the time-resolved electron temperature from the FastOES setup serves as a fundamental validation of our results.

## A. First Operating Condition: 150 V/0.98 A Discharge with 1.8 A Magnet Current

The first operating condition explored is one that produced relatively coherent breathing mode oscillations in the discharge current. The discharge voltage and current were 150 V and 0.98 A, about a quarter of the nominal operating power. The magnet current was 1.8 A, about twice as much as the discharge current. Nominally, the magnet current is about the same as the discharge current, but it was increased relative to the discharge current to achieve an oscillatory condition. The time-resolved discharge current and neutral emission lines for this condition are shown in Figure 4.

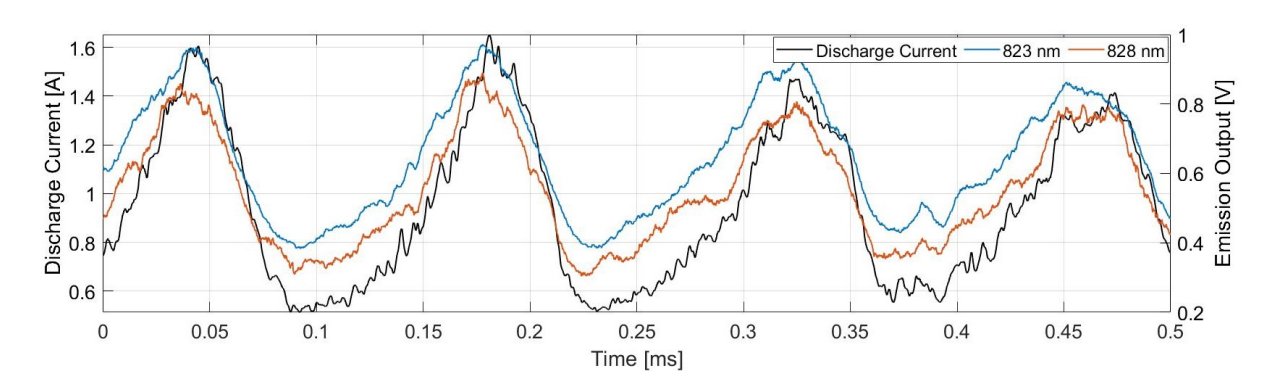


Fig. 4 Time-resolved discharge current and neutral emission lines for Operating Condition 1.

The discrete signals are transferred into the frequency domain via a Fast Fourier Transform (FFT). The FFTs of the discharge current and emitted light signals are shown in Figure 5. The primary breathing mode frequency appears at 7.34 kHz and has a relatively narrow bandwidth with a sharp peak. The first two harmonics are also visible, indicating that this is a coherent mode.

To determine the time-resolved electron temperature, the calibrated  $I_{823nm}/I_{828nm}$  line ratio is calculated. Then, assuming an electron density of  $3x10^{17}m^{-3}$ , a value reasonable for the discharge of this low-power thruster, the best fit electron temperature is found for each point in time. A moving average is applied to the resulting time-resolved electron temperature to eliminate erroneous spikes that are the result of noise in the data. The resulting time-resolved electron temperature for this condition is shown in Figure 6. The steady-state electron temperature, determined by the  $I_{823nm}/I_{828nm}$  line ratio measured by a spectrometer is shown in a red dashed line for reference. The general agreement between this value and the mean value of the time-resolved electron temperature gives us confidence that the FastOES setup provides a mean result that is close to that produced by known methods.

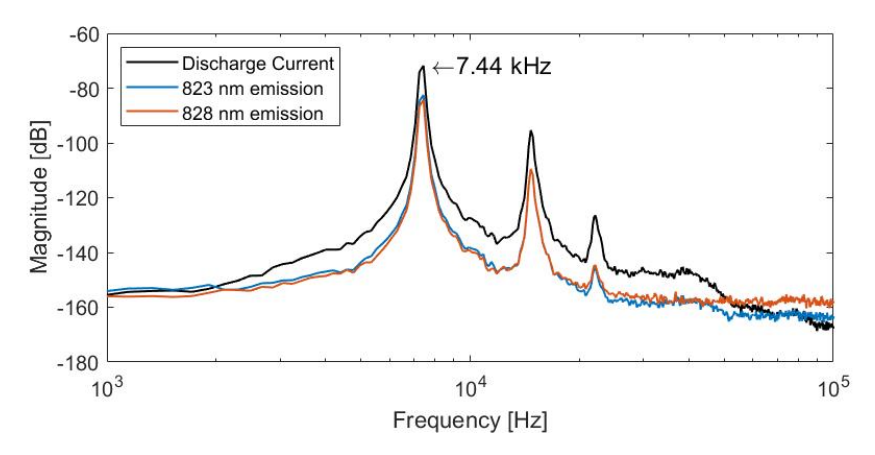


Fig. 5 FFT of time-resolved discharge current and neutral emission lines for Operating Condition 1.

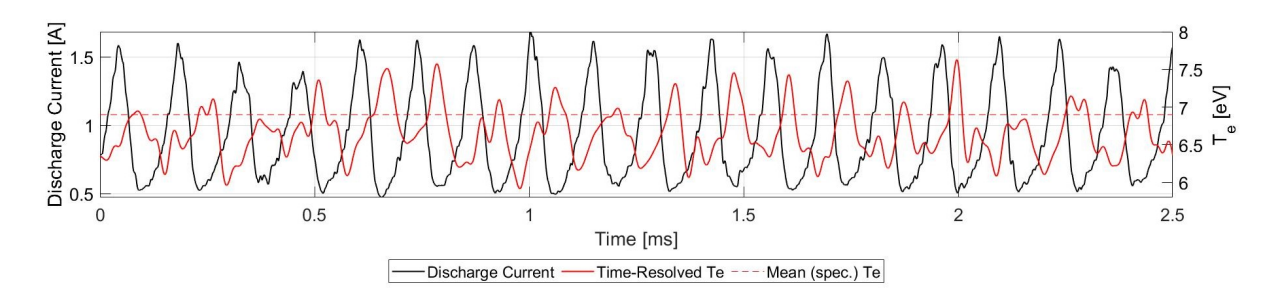


Fig. 6 Time-resolved discharge current and electron temperature for Operating Condition 1.

The resulting time-resolved electron temperature has a mean value of approximately 6.8 eV and an oscillation amplitude of 1 eV. The discharge current oscillations are centered around 0.98 A, with an amplitude of roughly 1A. Notably, the electron temperature appears to be out of phase with the discharge current, lagging by about 160 degrees. The remainder of this section will delve into the time-resolved electron temperature under two additional operating conditions, and discuss any discernible patterns.

# B. Second Operating Condition: 150 V/1.8 A Discharge with 1.8 A Magnet Current

The second operating condition examined maintained a discharge current of 150 V, but features a higher discharge current of 1.8 A to align with the magnet current of 1.8 A. This led to less coherent breathing mode oscillations. Figure 7 displays the time-resolved neutral emission lines, and Figure 8 illustrates the corresponding FFTs of these signals.

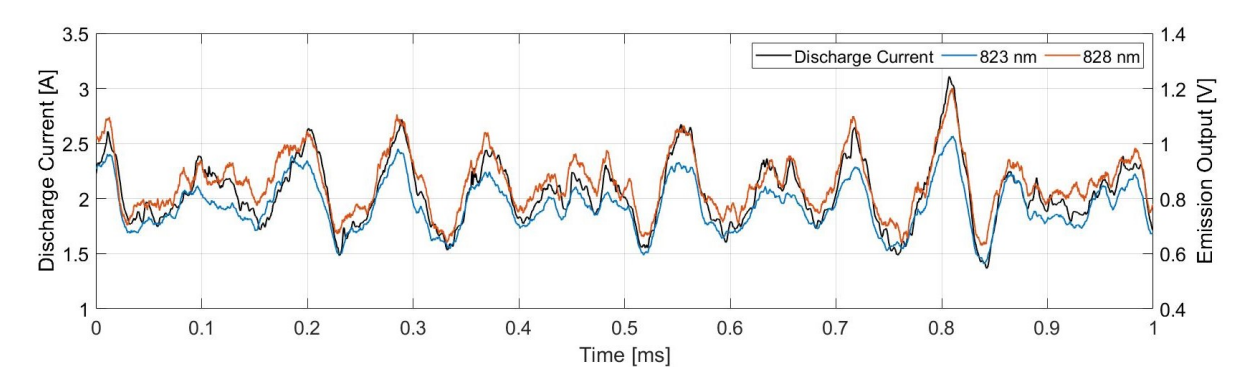


Fig. 7 Time-resolved discharge current and neutral emission lines for Operating Condition 2.

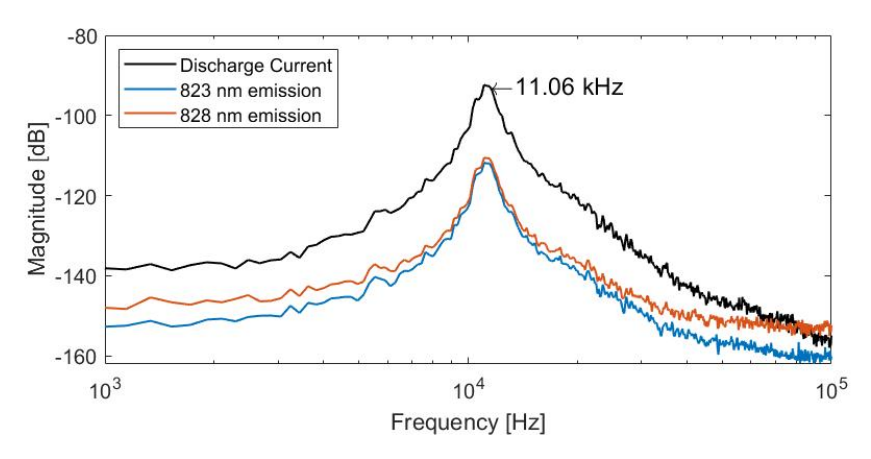


Fig. 8 FFT of time-resolved discharge current and neutral emission lines for Operating Condition 2.

In these figures, we note that the amplitude of oscillations in the discharge current spans approximately from 0.15 A to 1.1 A. The primary frequency of these oscillations is 11.44 kHz. Comparing the FFT in Fig. 8, to the FFT of the first operating condition, the frequency peak is broader, and no harmonics are observed, indicating a less coherent mode. Nevertheless, we can still determine the time-resolved electron temperature using the same method, as depicted in Fig. 9.

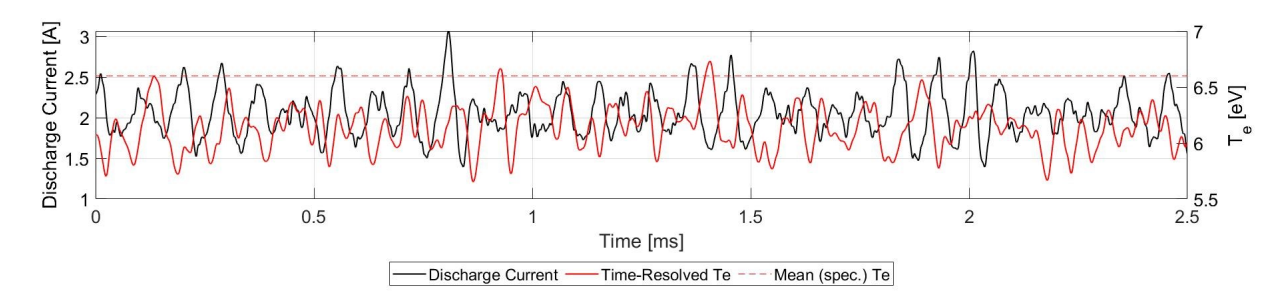


Fig. 9 Time-resolved discharge current and electron temperature for Operating Condition 2.

The mean time-resolved electron temperature is around 6.2 eV, with an amplitude ranging from 0.2 eV to 1 eV. Once again, we observe the electron temperature to be approximately out of phase with the discharge current. Although this mode is less coherent, the smaller features present in the time series are more apparent. Notably, at approximately 0.65 ms, a double peak is present in the discharge current oscillation. This double peak becomes evident in the electron temperature about 50  $\mu$ s later, at 0.7 ms. This corresponds to a phase delay of about 205 degrees. The same double peak is also apparent at 0.67 ms in the time-resolved emission signals in Fig. 7.

## C. Third Operating Condition: 250 V/0.8 A Discharge with 2A Magnet Current

The final mode explored involves a discharge voltage of 250 V, a discharge current of 0.8 A, and a magnet current of 2 A. In this configuration, characterized by higher discharge voltage and lower discharge current, the discharge current oscillations exhibit a slightly elevated and broader frequency peak at 14.59 kHz, with the oscillation amplitude ranging from 0.05 A to 0.25 A. The resulting electron temperature is centered around 7.25 eV, with the amplitude of oscillations spanning from 0.15 to 1.25 eV. Figures 10 and 11 present FFTs of the signals and time-resolved electron temperature, respectively.

Despite the diminished coherence in this mode, a notable observation persists: the electron temperature consistently lags behind the discharge current. Section VI will delve into the factors contributing to this phenomenon, offering comparisons with findings from prior studies on breathing mode behaviors. Additionally, we will discuss common patterns observed across all three result cases to draw broader insights. This exploration aims to provide a comprehensive understanding of the observed dynamics and their implications for the broader understanding of Hall thruster behavior.

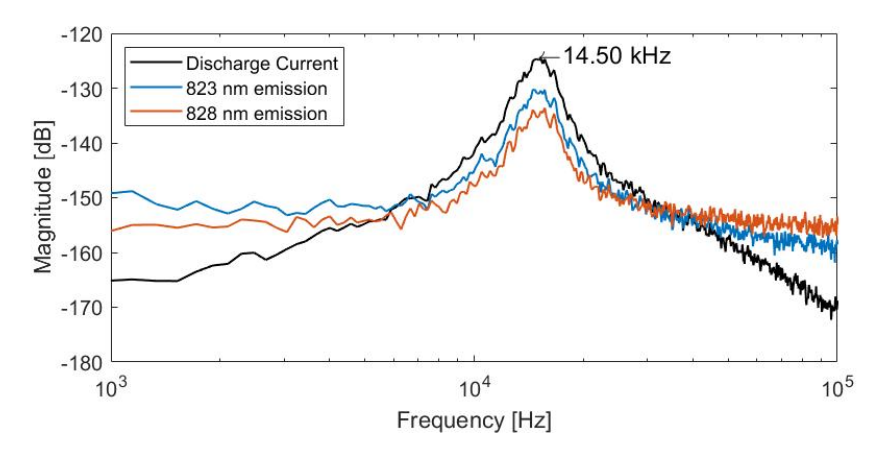


Fig. 10 FFT of time-resolved discharge current and neutral emission lines for Operating Condition 3.

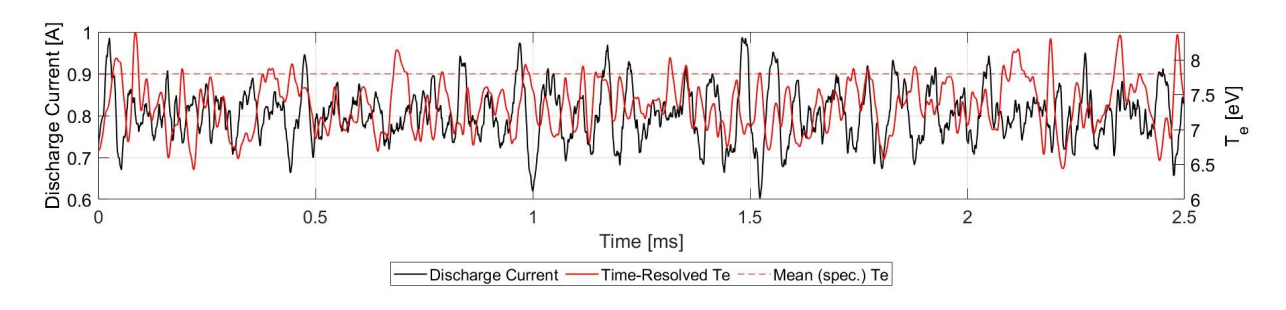


Fig. 11 Time-resolved discharge current and electron temperature for Operating Condition 3.

#### D. Summary of results

Table 1 provides a concise overview of the thruster operating conditions, mean electron temperature, main frequency and amplitude of the discharge current and electron temperature oscillations. It also includes the amplitude of discharge current and electron temperature oscillations, normalized by their respective mean values. It is important to note that the exact amplitude of electron temperature variations may be influenced by assumptions about electron density or the nature of the moving average applied to the raw optical data, further discussed in Section VI. To determine the oscillation amplitude, the local minima and maxima of the time-resolved signals were identified and the differences between them were calculated. Then, all the calculated amplitudes were plotted in a histogram to observe the spread. In the first operating condition, the amplitude distribution was relatively narrow and centered around a single value. Conversely, the second and third operating conditions exhibited a broader amplitude spread, and thus an "amplitude range" is recorded.

There is marginal variation observed in the mean electron temperature among different operating conditions, although it remains relatively consistent. Notably, the peak-to-peak variations in electron temperature, when normalized by their mean value, seem to display a loose scaling relationship with peak-to-peak variations in the discharge current also normalized by their mean value. This trend is evident also in Fig. 6 and 9 which illustrate the time series of discharge current and electron temperature.

 Table 1
 Summary of Results

O.C. #	$V_D[V]$	$I_D[V]$	$I_{D,pk-pk}$ [A]	$\frac{I_{D,pk-pk}}{I_D}$	$T_e$ [eV]	$T_{e,pk-pk}$ [eV]	$\frac{T_{e,pk-pk}}{T_e}$	F [kHz]
						1		
2	150	1.8	0.15 - 1.1	0.08 - 0.6	6.2	0.2 - 1	0.03 - 0.16	11.44
3	250	0.8	0.05 - 0.25	0.06 - 0.3	7.25	0.15 - 1.25	0.02 - 0.17	14.6

## VI. Discussion

We hypothesized that the electron temperature undergoes temporal variations, a claim substantiated by our findings. Additionally, the expectation that the amplitude of these oscillations correlates with the amplitude of discharge current oscillations seems to hold true. However, we do note that the amplitude of electron temperature oscillations was relatively small. Exploring similar measurements in a Hall thruster characterized by higher amplitude and frequency discharge current oscillations would offer an intriguing avenue for future investigation.

Across all the investigated operating conditions explored in this study, the resulting time-resolved electron temperature consistently exhibited a strong correlation with the discharge current, in which the electron temperature exhibited an approximate phase lag behind the discharge current. A plausible physical explanation for this phase relationship between electron temperature and neutral density is that as the neutral density decreases, the electric field strengthens, leading to an increase in electron temperature. Consequently, the heightened electron temperature contributes to a higher ionization rate, further contributing to the decrease in neutral density [10]. This insight supports an anticipated anti-correlation between neutral density and electron temperature. Although we lack a direct measurement of neutral density, the intensity of emitted light is known to scale with neutral density, and thus may provide a proxy for the expected phasing. Additionally, the observed in-phase relationship between emission intensity and discharge current enables the use of discharge current as a reliable time reference. Therefore, the justification for the phase lag between the electron temperature and discharge current may be provided in this manner.

In considering the implications of these results on Hall thruster models and performance, it is evident that such fluctuations do exist, although perhaps on a small scale. Furthermore, these variations appear to scale with changes in discharge current. In a study examining the influence of electron mobility fluctuations on breathing mode oscillations [10], a case was tested in which a linear scale for electron temperature fluctuations proportional to those of neutral density was assumed. In light of our observations, adopting such an approach in modeling could be reasonable. However, further investigation is necessary to establish a comprehensive scaling law.

Several limitations are associated with our approach and findings. As is characteristic of optical emission spectroscopy measurements, the spatial resolution is constrained. Also, with the requirement of high speed measurements at specific wavelengths, the signal-to-noise ratio is relatively low. Moreover, there are several factors which could skew the amplitude of the measured electron temperature oscillations. First, the derived electron temperature hinges on an assumed electron density, which while we can provide a reasonable guess for this value, is not exactly known. However, a brief sensitivity analysis indicated that assuming a higher electron density within an order of magnitude does not substantially affect the oscillation amplitude but primarily results in a decrease in the mean value around which the oscillations are centered. Another potential source of error is that the 823.2 nm line, whose upper level is populated by a metastable state, may not respond quickly enough to changes in plasma parameters. Furthermore, the selected averaging or smoothing method applied to the emission data has the potential to impact the resulting amplitude. In particular, oversmoothing the data may lead to an underestimated amplitude. Despite these limitations, we address them to the best of our ability, and our study nonetheless provides valuable insights into the understanding of electron temperature dynamics in this context.

#### VII. Conclusion

This investigation of a low-power Hall thruster reveals that the amplitude of electron temperature oscillations, although modest, appears to correlate with the amplitude of discharge current oscillations typically associated with the breathing mode. Furthermore, these electron temperature oscillations exhibit an approximate out-of-phase relationship, a correlation supported by the anticipated phase dynamics with the neutral density and electron temperature. While the electron temperature may not be the driving cause of the onset and maintenance of the breathing mode in all cases, it does emerge as a discernible feature of the breathing mode that our FastOES diagnostic captures effectively. The outcomes of this study lend support to the concept of a non-constant electron temperature in Hall thruster models, potentially linked to neutral density oscillations.

#### VIII. Future Work

In continuing research efforts with the FastOES diagnostic, a key improvement could be made in addressing spatial resolution limitations. One approach to this could be leveraging the CRM's ability to calculate the total intensity of light emitted for given plasma parameters. By employing the CRM to compute the emitted light intensity along discrete points in a line of sight, utilizing expected plasma parameters derived from simulations, we could gain a better

understanding of light distribution in difficult-to-access areas like the discharge channel. This approach allows us to test the assumption that the brightest part of the line of sight will dominate the measurements and help to understand exactly where this brightest part is located. Experimentally validating this assumption could involve directing the collection optic at the same location for various entrance angles, subsequently assessing changes in total intensity and spectra across the range of angles.

Also, a broader range of Hall thruster operating conditions could be explored to comprehensively examine scaling relationships. Specifically, the focus would be on identifying modes exhibiting distinct breathing mode oscillations to evaluate whether the amplitude of oscillations scales with specific thruster parameters. Additionally, an extension of the current study could involve investigating how the phasing and oscillation amplitude vary spatially across different regions of the thruster plume.

A further extension of this research could involve similar investigations with different Hall thruster classes, such as high-power thrusters or magnetically shielded designs. Exploring high-power Hall thrusters may reveal higher amplitude oscillations and higher breathing mode frequencies. Also for regimes with higher electron density, it may be appropriate to use the xenon ion 441.5 nm to 605.2 nm line ratio which has been shown to have a better time response than the neutral xenon 823.2 nm to 828 nm line ratio.

# Acknowledgments

This research was carried out in collaboration between the University of California, Los Angeles (UCLA) and employees of the Jet Propulsion Laboratory, California Institute of Technology (JPL). This research was carried out at the Jet Propulsion Laboratory, California, under a contract with the National Aeronautics and Space Administration. We gratefully acknowledge support from the NASA Space Technology Graduate Research Fellowship (grant number 80NSSC19K117) and the DOE Award DE-AR0001378, "AMPERE: Advanced Materials for Plasma Exposed Robust Electrodes". We also thank and acknowledge Vernon Chaplin for sharing the Xe I collisional-radiative model and Robert Lobbia for his role in the initial development of the FastOES diagnostic.

## References

- [1] Fife, J., Martinez-Sanchez, M., and Szabo, J., "A numerical study of low-frequency discharge oscillations in Hall thrusters," 33rd Joint Propulsion Conference and Exhibit, American Institute of Aeronautics and Astronautics Inc, AIAA, 1997. https://doi.org/10.2514/6.1997-3052.
- [2] Dale, E., and Jorns, B., "Two-zone Hall thruster breathing mode mechanism, Part I: Theory," *36th International Electric Propulsion Conference, Vienna, Austria*, IEPC-2019-354.
- [3] Dale, E., and Jorns, B., "Two-zone Hall thruster breathing mode mechanism, Part II: Experiment," 36th International Electric Propulsion Conference, Vienna, Austria, IEPC-2019-352.
- [4] Barral, S., and Ahedo, E., "Low-frequency model of breathing oscillations in Hall discharges," *Physical Review E*, Vol. 79, 2009. https://doi.org/10.1103/PhysRevE.79.046401.
- [5] Raisanen, A., Hara, K., and Boyd, I., "Two-dimensional hybrid-direct kinetic simulation of a Hall thruster discharge plasma," *Physics of Plasmas*, Vol. 26, 2019. https://doi.org/10.1063/1.5122290.
- [6] Hara, K., Boyd, I., and Kolobov, V., "One-dimensional hybrid-direct kinetic simulation of the discharge plasma in a Hall thruster," *Physics of Plasmas*, Vol. 19, 2012. https://doi.org/10.1063/1.4768430.
- [7] Hara, K., Sekerak, M., Boyd, I., and Gallimore, A., "Pertubation analysis of ionization oscillations in Hall effect thrusters," *Physics of Plasmas*, Vol. 21, 2014. https://doi.org/10.1063/1.4903843.
- [8] Dale, E., Hara, K., and Jorns, B., "Numerical investigation of the stability criteria for the breathing mode in Hall Effect Thrusters," *35th International Electric Propulsion Conference, Atlanta, GA*, IEPC-2017-265.
- [9] Lafleur, T., Chabert, P., and Bourdon, A., "The origin of the breathing mode in Hall thrusters and its stabilization," *Journal of Applied Physics*, Vol. 130, 2021. https://doi.org/10.1063/5.0057095.
- [10] Leporini, L., Giannetti, V., Saravia, M., Califano, F., Camarri, S., and Andreussi, T., "On the onset of breathing mode in Hall thrusters and the role of electron mobility flucturations," *Frontiers in Physics*, Vol. 10, 2022. https://doi.org/10.3389/fphy.2022. 951960.

- [11] Sullivan, R. M., Yost, A., and Johnson, L. K., "Near-Field Angular Distributions of High Velocity Ions for Low-Power Hall Thrusters," *IEEE Aerospace Conference*, IEEE, Big Sky, MT, 2009. https://doi.org/10.1109/AERO.2009.4839594.
- [12] Konopliv, M., Johnson, L., Chaplin, V., Lobbia, R., Thuppul, A., Simka, T., and Wirz, R., "Collisional-Radiative Models of Neutral and Singly-Ionized Xenon in Hall Thrusters: Experimental Validation and Model Investigations," AIAA Propulsion and Energy Forum and Exposition, submitted for publication 2021. https://doi.org/https://doi.org/10.2514/6.2021-3390.
- [13] Nakles, M., and Matlock, T., "Hall Thruster Near-Field Plume Characterization Through Optical Emission Spectroscopy," 36th International Electric Propulsion Conference, Vienna, Austria, IEPC-2019-246. https://doi.org/https://doi.org/10.2514/6.2021-3378.
- [14] Konopliv, M., Simka, T., Lobbia, R., Johnson, L., and Wirz, R., "Fast Optical Emission Spectroscopy for Studying Plasma Behavior in Hall Thrusters," 37th International Electric Propulsion Conference, Cambridge, MA, IEPC-2022-171.
- [15] Chaplin, V., Johnson, L., Lobbia, R., Konopliv, M., Simka, T., and Wirz, R., "Insights from Collisional-Radiative Models of Neutral and Singly-Ionized Xenon in Hall Thrusters," *AIAA Propulsion and Energy Foruum and Exposition*, submitted for publication 2021.
- [16] Karabadzhak, G. F., Chiu, Y.-H., and Dressler, R. A., "Passive optical diagnostic of Xe-propelled Hall thrusters. II. Collisional-radiative model," *Journal of Applied Physics*, Vol. 99, No. 11, 2006, p. 113305. https://doi.org/10.1063/1.2195019.